

OPEN ACCESS

EDITED BY Iseli L. Nantes, Universidade Federal do ABC, Brazil

REVIEWED BY
Paula Haddad,
Universidade Federal de Sao Paulo, Brazil
Aryane Tofanello,
Federal University of ABC, Brazil

*CORRESPONDENCE Vugar Yagublu, ☑ vugar.yagublu@umm.de

[†]These authors have contributed equally to this work

RECEIVED 23 May 2025 ACCEPTED 08 September 2025 PUBLISHED 22 September 2025

CITATION

Karimova A, Hajizada S, Shirinova H, Nuriyeva S, Gahramanli L, Mehdiyeva A, Eyvazova G, Sadikhov T, Lenz N, Nasirova I, Reissfelder C and Yagublu V (2025) Dextran-coated Fe_3O_4 nanoparticles with ratio-dependent drug loading: structural characterization and cytotoxicity in colorectal cancer cells. Front. Nanotechnol. 7:1634225. doi: 10.3389/fnano.2025.1634225

COPYRIGHT

© 2025 Karimova, Hajizada, Shirinova, Nuriyeva, Gahramanli, Mehdiyeva, Eyvazova, Sadikhov, Lenz, Nasirova, Reissfelder and Yagublu. This is an open-access article distributed under the terms of the Creative Commons Attribution License (CC BY). The use, distribution or reproduction in other forums is permitted, provided the original author(s) and the copyright owner(s) are credited and that the original publication in this journal is cited, in accordance with accepted academic practice. No use, distribution or reproduction is permitted which does not comply with these terms.

Dextran-coated Fe₃O₄ nanoparticles with ratio-dependent drug loading: structural characterization and cytotoxicity in colorectal cancer cells

Aynura Karimova^{1,2†}, Sabina Hajizada^{3,4†}, Habiba Shirinova⁵, Sevinj Nuriyeva¹, Lala Gahramanli¹, Aygun Mehdiyeva⁵, Goncha Eyvazova¹, Toghrul Sadikhov⁶, Natalia Lenz⁷, Inji Nasirova⁴, Christoph Reissfelder³ and Vugar Yagublu^{3*}

¹Nanoresearch Laboratory, Baku State University, Baku, Azerbaijan, ²Department Chemistry of High Molecular Weight Compounds, Baku State University, Baku, Azerbaijan, ³Department of Surgery, Medical Faculty Mannheim, University of Heidelberg, Mannheim, Germany, ⁴Scientific Research Centre, Azerbaijan Medical University, Baku, Azerbaijan, ⁵Department of Chemical Physics of the Nanomaterials, Baku State University, Baku, Azerbaijan, ⁶Department of Molecular Biology and Genetics, Institute of Graduate Studies In Sciences, Istanbul University, Istanbul, Türkiye, ⁷Faculty of Medicine, Philipps-University Marburg, Marburg, Germany

Introduction: This study focuses on the development of dextran-coated iron oxide nanoparticles (Fe_3O_4 @Dextran NPs) as carriers for chrysin, a natural flavonoid with recognized anticancer activity.

Methods: Fe $_3$ O $_4$ @Dextran NPs were synthesized via co-precipitation and loaded with chrysin at different drug-to-nanoparticle ratios. Structural and physicochemical characterization was performed using X-ray Diffraction (XRD), Fourier Transform Infrared Spectroscopy (FTIR), and Vibrating Sample Magnetometry (VSM). Drug loading efficiency was determined spectrophotometrically. The anticancer efficacy of the drug-loaded samples was assessed *in vitro* against HCT-116 human colorectal carcinoma cells using the MTT assay, with statistical analysis performed by one-way ANOVA.

Results: XRD revealed an average crystallite size of 17 nm for Fe $_3$ O $_4$ @Dextran, which decreased to ~15 nm upon chrysin loading. FTIR confirmed the successful incorporation of chrysin without compromising structural stability. VSM measurements demonstrated superparamagnetic behavior with a saturation magnetization of 69.2 emu/g. Drug loading efficiencies were 42%, 54%, and 57% at drug-to-nanoparticle ratios of 1:0.5, 1:1, and 1:2, respectively, with evidence of saturation at higher concentrations. The Fe $_3$ O $_4$ @Dextran+D2 formulation exhibited optimal drug loading, maintaining structural integrity and enhanced cytotoxic activity against HCT-116 cells.

Conclusion: Fe_3O_4 @Dextran+D2 demonstrated favorable structural integrity (as evidenced by XRD and FTIR analyses) along with notable anticancer activity

against HCT-116 cells. Its performance is attributed to optimal drug loading without surface saturation, supporting its potential as a structurally stable drug delivery system.

KEYWORDS

iron oxide nanoparticles, dextran coating, tumor microenvironment, surface modification, drug carriers

1 Introduction

Magnetic nanoparticles (MNPs), particularly iron oxide nanoparticles (Fe₃O₄ NPs), have garnered increasing attention as promising materials for the development of effective anticancer therapeutics and diagnostic tools (Ramazanov et al., 2021; Mamani et al., 2023). The growing interest in MNPs can be attributed to their unique physicochemical characteristics, such as superparamagnetism, large surface-to-volume ratio, controllable size, and ease of surface modification (Zhu et al., 2018; Ramazanov et al., 2020; Ezealigo et al., 2021; Pozzi et al., 2024). In particular, the ability to design these NPs with tailored functionalities and chemically modified surfaces has led to significant advancements in the field of multifunctional nanocarriers (Akbarzadeh et al., 2012; Huang et al., 2016; Mosayebi et al., 2017; Ali et al., 2021; Pusta et al., 2023; Sala et al., 2023; Stiufiuc and Stiufiuc, 2024).

Recent advances have expanded the applications of MNPs beyond conventional imaging and drug delivery. For instance, functionalized glucose oxidase-loaded iron-based nanoparticles (Gox@Fe NPs) enable photothermal-ferroptosis combined with PD-L1 immunotherapy and magnetic resonance imaging (MRI)-guided tumor ablation (Li et al., 2024). Another promising direction involves incorporating Fe₃O₄ NPs into alginate hydrogels for nearinfrared (NIR) light-triggered photothermal therapy of colorectal cancer (Ji and Wang, 2023) the development of superparamagnetic polycrystalline Fe₃O₄ superparticles (Attanayake et al., 2025), which consist of 10–15 nm nanocrystals aggregated into 160–400 nm clusters, revealed specific absorption rates exceeding 250 W/g at a low concentration (0.5 mg/mL) in an 800 Oe, 310 kHz alternating field, highlighting their potential for low-dose magnetic hyperthermia.

Despite these advantages, MNPs also face several limitations, including low aggregation stability and weak covalent interactions with surface modifiers. Due to the high surface area and dipole-dipole interactions, Fe₃O₄ NPs tend to agglomerate, leading to increased particle size and enhanced uptake by the reticuloendothelial system (RES) *in vivo* (Chuan Lim and Feng, 2012; Zein et al., 2020).

To address these challenges, numerous studies have explored the functionalization of ${\rm Fe_3O_4}$ NPs (Yan et al., 2009; Liu et al., 2020). To confer intriguing physicochemical properties, the surface of ${\rm Fe_3O_4}$ NPs has been coated with various polymers, inorganic materials, and biological molecules (Zhu et al., 2018; Liu et al., 2020).

In our previous work, we studied the effects of chitosan and polyethylene glycol (PEG) coatings on the structural characteristics, drug-loading efficiency, and anticancer efficacy of chrysin-loaded Fe₃O₄ NPs, demonstrating that PEG-coated NPs exhibited superior loading efficiency, enhanced structural stability, and improved antitumor activity compared to chitosan-coated formulations (Karimova et al., 2024).

Building on these findings, the current work explores the use of dextran as an alternative coating material for Fe $_3$ O $_4$ NPs. While PEG and chitosan are well-recognized biopolymer coatings, exploring various biopolymer coatings is crucial for systematically investigating how the nature of the coating impacts the structural profile and functional performance of Fe $_3$ O $_4$ NPs. Different polymers interact variably with the NP surface and the drug molecule, potentially affecting crystal structure, particle size, drug loading efficiency, and biological activity. By utilizing dextran as a coating material, this research aims to explore how such variations influence structure-property relationships and anticancer potential through detailed structural, functional, and cytotoxicity analyses.

Dextran, a hydrophilic and biocompatible polysaccharide with a flexible molecular structure, has been widely used in biomedical applications, including as a stabilizer for MNPs and a platform for drug delivery. Due to its unique molecular architecture and interaction profile, dextran can be employed to investigate structure-property relationships and optimize nanocarrier behavior in terms of drug loading efficiency and cytotoxicity.

In this study, we employed dextran as a coating material for $\rm Fe_3O_4$ NPs, while chrysin, a natural flavonoid compound with anticancer properties, served as the representative drug molecule (Sood et al., 2024). By comparing the structural characteristics, drug-loading efficiency, and cytotoxicity in relation to our earlier PEG-and chitosan-based formulations, we aim to contribute to a broader understanding of how coating composition influences system functionality and aids in the optimized design of advanced nanocarriers.

2 Materials and methods

2.1 Materials

Ferric chloride hexahydrate (FeCl₃·6H₂O, 98%), ferrous sulfate heptahydrate (FeSO₄·7H₂O, 98%), and ammonium hydroxide solution (NH₄OH, 23%–25%) were utilized for the coprecipitation synthesis of Fe₃O₄ NPs. Dextran (($C_6H_{10}O_5$)_n, M_r~40000) served as the surface-modifying agent. Chrysin ($C_{15}H_{10}O_4$, 97%) was employed as an anticancer drug, and dimethyl sulfoxide (DMSO, (CH₃)₂SO, \geq 99.7%) was used as a solvent. All chemicals were used directly without further purification.

2.2 Methods

2.2.1 Preparation of Fe₃O₄@Dextran NPs

 $Fe_3O_4@Dextran\ NPs\ were\ synthesized\ via\ the\ co-precipitation\ method\ described\ in\ previous\ work\ (Karimova\ et\ al.,\ 2024).\ Briefly,\ a$

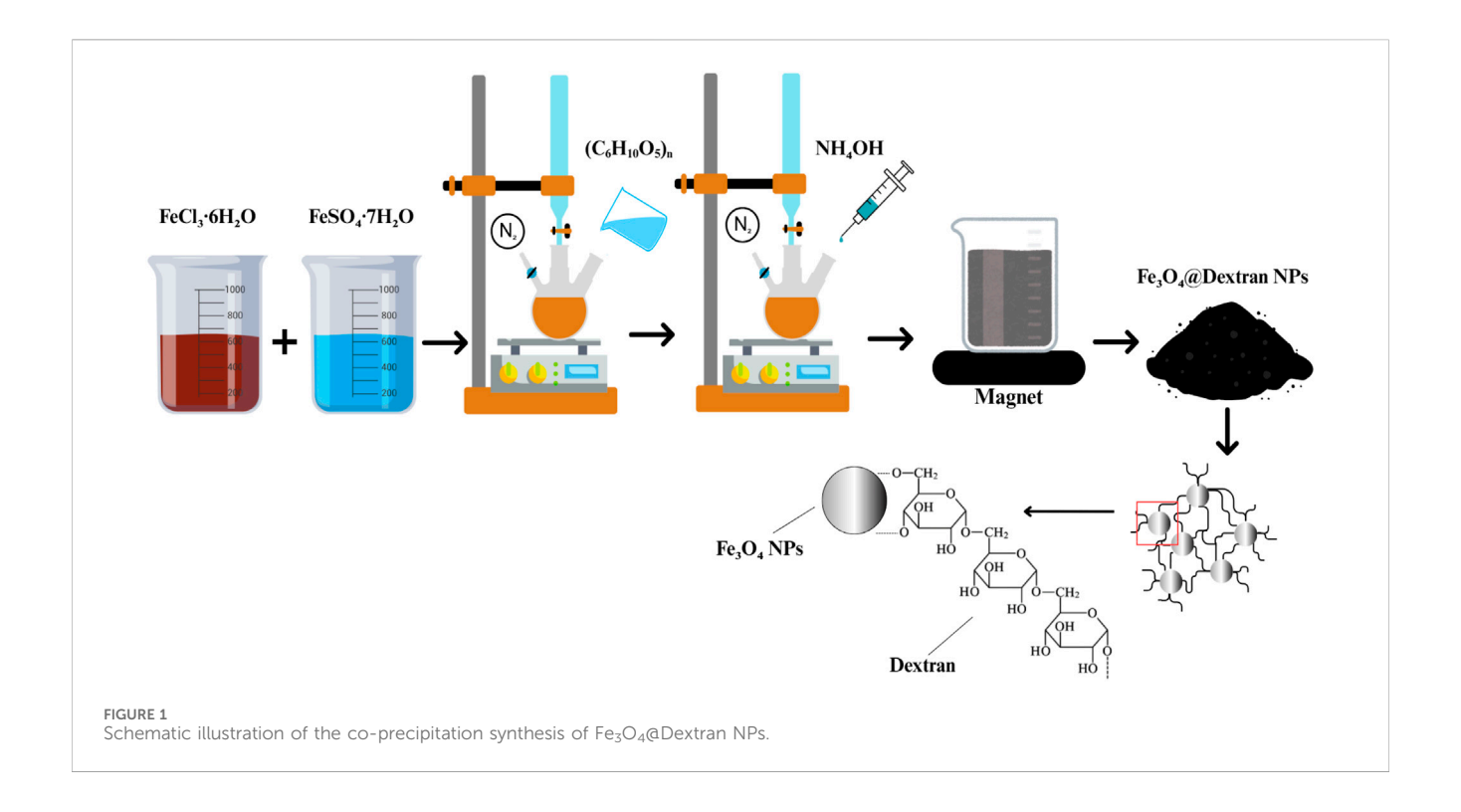


TABLE 1 The composition of drug-loaded Fe $_3$ O $_4$ @Dextran NPs. While obtaining the samples, the amount of Fe $_3$ O $_4$ @Dextran NPs remained constant at 100 mg, while the amount of drug loaded into the NPs varied at three different ratios: 1:0.5, 1:1, and 1:2.

Samples	Fe ₃ O ₄ @Dextran NPs (mg)	Drug (mg)	Ratio of Fe₃O₄@Dextran NPs to drug
Fe ₃ O ₄ @Dextran + D1	100	50	1:0.5
Fe ₃ O ₄ @Dextran + D2	100	100	1:1
Fe ₃ O ₄ @Dextran + D3	100	200	1:2

homogeneous solution of $FeCl_3 \cdot 6H_2O$ and $FeSO_4 \cdot 7H_2O$ in a molar ratio of 2:1 was prepared in 100 mL of deionized water and stirred at a rate of 400 rpm (Figure 1).

The solution was then heated to 70 °C for 30 min under a nitrogen (N_2) atmosphere to eliminate dissolved oxygen (O_2) and prevent the unwanted oxidation of Fe₃O₄ to γ -Fe₂O₃.

To stabilize the NPs, 8 g of dextran was slowly added to the solution, and stirring continued for approximately 1 h to ensure proper coating of the NPs during their formation. Subsequently, 10–15 mL of NH₄OH (23%–25%) was added dropwise under vigorous stirring until the pH reached and was maintained at approximately 10. A black precipitate formed immediately upon stirring. The principal reaction is:

$$Fe^{2+} + 2Fe^{3+} + 8OH^{-} \rightarrow Fe_3O_4 \downarrow + 4H_2O$$
 (1)

To control the mean size of the NPs, the temperature and pH of the solution were continuously monitored during synthesis (Wu et al., 2015). Finally, the temperature was increased to 90 °C, and the reaction was allowed to continue for an additional hour while being vigorously stirred at a rate of 400 rpm. The final pH of the solution was approximately 10. After the reaction, the beaker containing the suspension was placed on a NdFeB magnet. The supernatant was

removed, and the precipitate was washed with deionized water several times until the final decanted water became neutral. Finally, the dextran-coated Fe $_3$ O $_4$ (Fe $_3$ O $_4$ @Dextran) NPs were placed in an oven and dried for 4 h at 80 °C.

2.2.2 Loading of drug

The loading of chrysin into the Fe₃O₄@Dextran NPs was performed using the physical adsorption method, a simple, and non-destructive approach that preserves the structural integrity of both the NPs and the drug. Briefly, chrysin was solubilized in DMSO and then added to the Fe₃O₄@Dextran powder. The mixture was stirred with a mechanical stirrer at 700 rpm for 6 h at room temperature. At the end of the procedure, the drug-loaded Fe₃O₄@Dextran NPs were removed from the solution by centrifugation at 15,000 rpm and washed with deionized water to eliminate weakly adsorbed drug on the surface. Subsequently, the chrysin-loaded samples were dried in an oven at 40 °C for 4 h.

In this work, the effect of drug concentration on drugloading efficiency was investigated. To achieve this, the chrysin concentration was adjusted to different amounts (Table 1).

2.2.3 Characterization techniques

The structure, chemical characterization, and drug-loading efficiency of the Fe₃O₄@Dextran NPs were investigated using X-ray diffraction (XRD), Fourier-transform infrared (FTIR) spectroscopy, and ultraviolet-visible (UV-Vis) spectroscopy. XRD analysis was conducted using a Rigaku Mini Flex 600 X-ray diffractometer operating in reflection mode with high-intensity Cu- $K\alpha$ radiation and a 2θ range of $20^{\circ}-80^{\circ}$ to analyze the crystallinity and size of the samples. The molecular structure of the dextran-coated NPs was examined using a Varian 3600 FTIR spectrometer with KBr pellets, with the spectrum observed from 3,400 to 600 cm⁻¹. The magnetic properties of the samples were investigated using a Superconducting Quantum Interference Device (SQUID) magnetometer (MPMS), with magnetic characterization performed over a temperature range of 5-300 K and under applied magnetic fields up to ±5 T. Additionally, the drug-loading efficiency for all samples was assessed using a Specord250 PLUS UV-Vis spectrometer.

2.2.4 Calculation of drug-loading efficiency

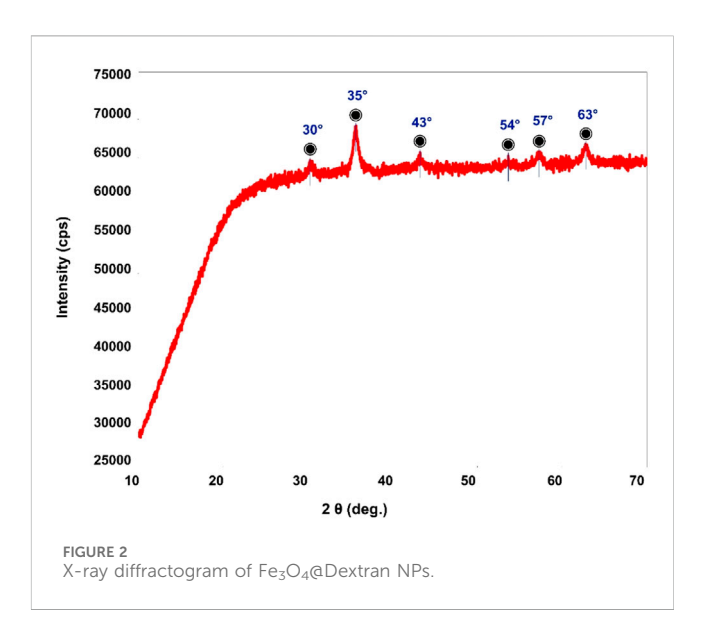
The drug loading efficiency (LE%) of chrysin onto Fe₃O₄@ Dextran NPs was calculated by measuring the concentration of chrysin remaining in the supernatant after centrifugation (10 min at 15000 rpm). The amount of free drug in the supernatant was quantified using UV-Vis spectroscopy, with absorbance measured at 276.4 nm. The LE% was determined by removing the amount of free chrysin (D_{Free}) remaining in the supernatant after centrifugation from the total amount of chrysin (D_{Total}) in the suspension. The drug LE (%) was calculated using the following equation:

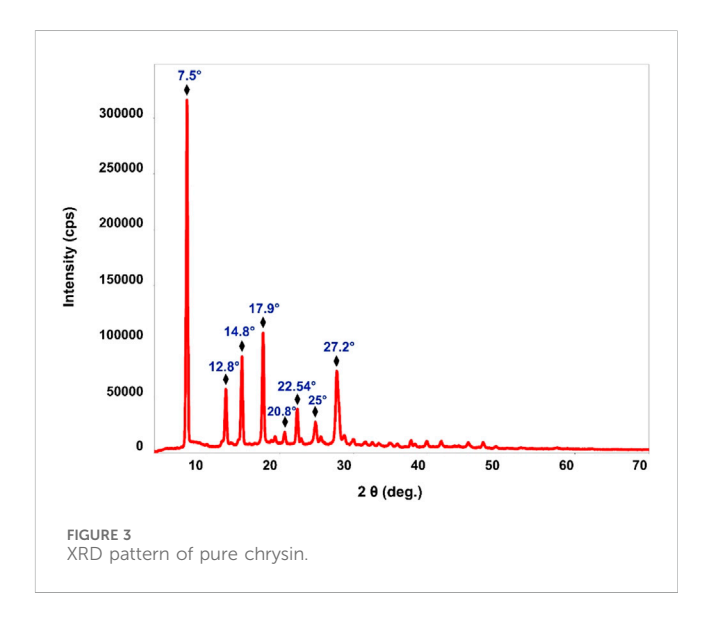
$$LE = \frac{D_{Total} - D_{Free}}{D_{Total}} \times 100\% \tag{2}$$

This method was adapted from a previously reported technique (Sood et al., 2024).

2.2.5 Cell culture and MTT assay

The anti-cancer efficacy of the selected Fe₃O₄ NPs was evaluated using HCT 116 human colon cancer cells. To dissolve the various Fe₃O₄ NPs, DMSO was used as a solvent due to its high solubility for hydrophobic drugs such as chrysin, facilitating effective cell culture assays. Importantly, we adhered to standard cytotoxicity guidelines, maintaining DMSO concentrations consistently below 0.1% to prevent potential solvent-induced cytotoxicity, as supported by existing literature (Zhang et al., 2017). Studies have demonstrated that DMSO concentrations below 0.1% have negligible effects on cell viability, thus validating our approach (Baldelli et al., 2021). HCT 116 cells were maintained in Dulbecco's Modified Eagle Medium (DMEM) supplemented with 10% Fetal Bovine Serum (FBS) and 1% penicillin-streptomycin-neomycin (PSN) under a humidified atmosphere (5% CO₂) at 37 °C. Once 75%-80% confluence was achieved, the cells were re-equilibrated with trypsin (0.25%) and EDTA (0.52 mM) in phosphate-buffered saline (PBS) and harvested at the appropriate density for 24 h before the cell viability assessment. In this assay, the HCT 116 cells were treated with chrysin-loaded Fe₃O₄ NPs coated with dextran at varying concentrations (0-40 µg/mL) for 24 h. After treatment, the cells were rinsed with PBS, and MTT solution was added to form

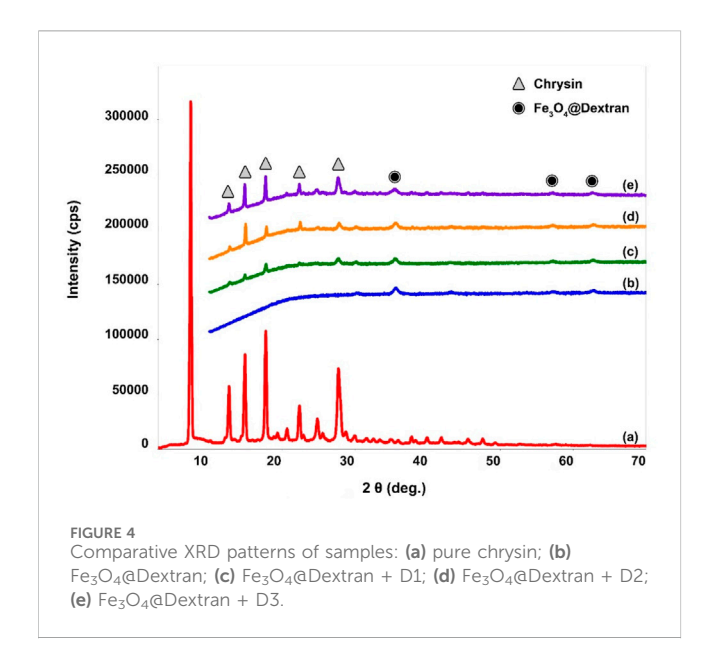




formazan salt. Subsequently, the media were replaced with DMSO (200 $\mu L)$ to dissolve the formed formazan crystals in each well. The viability of the cells was spectrophotometrically determined at 570 nm using an ELISA reader (Emax, Molecular Devices, San Jose, CA, United States of America) to assess the number of viable cells. All treatment experiments were performed in triplicate.

2.2.6 Statistical analysis

Statistical analyses were conducted using JMP software version 16 (SAS Institute Inc., Cary, NC, United States) and GraphPad Prism Software version 10.0.0 for Windows, GraphPad Software, Boston, Massachusetts, United States. The differences among multiple groups were analyzed using one-way ANOVA, followed by Tukey's method for post-hoc comparisons. Differences with p < 0.05 were considered statistically significant (JMP). GraphPad Prism Software was used for graphical visualization.



2.2.7 Declaration of generative AI in writing this manuscript

The manuscript creation process did not utilize any artificial intelligence tools for developing ideas, generating text, or improving content quality. For grammatical accuracy and language refinement, conventional writing tools such as Grammarly were employed.

3 Results

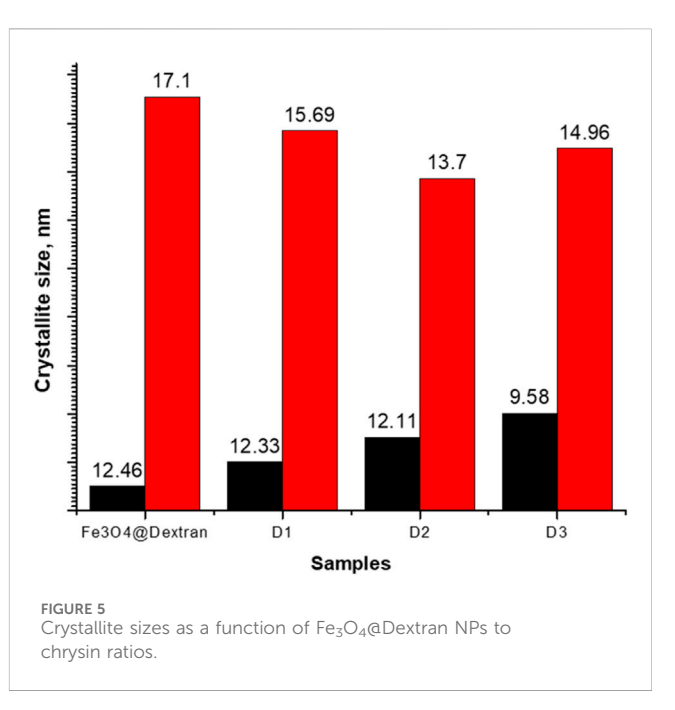
3.1 XRD analysis

Figure 2 shows the XRD pattern of Fe_3O_4 @Dextran NPs. The spectrum exhibited peak distribution typical of the face-centered cubic spinel structure of magnetite, with a major peak at ~35° corresponding to the (311) plane. Other peaks for this crystal structure were observed at 20 positions of ~30° (200), 43° (400), 54° (422), 57° (511), and 63° (440), which align well with those from the JCPDS card (19-0629). The low intensity of the peaks indicates the presence of amorphous dextran on the surface of the NPs. Furthermore, the average crystallite size of Fe_3O_4 @Dextran NPs was estimated to be about 12.46 nm–17.10 nm, calculated from X-ray line broadening using Scherrer's formula (Karimova et al., 2023).

The anticancer agent chrysin was loaded into the dextran-coated samples using a non-covalent method. For comparative purposes, X-ray structural analysis of pure chrysin was also performed (see Figure 3). Chrysin displayed sharp and intense peaks at 7.5°, 12.8°, 14.8°, 17.9°, 20.8°, 22.54°, 25°, and 27.2° as assessed via XRD analysis (Kaur et al., 2015). The crystalline nature of chrysin is evident from these distinct diffraction peaks, confirming that the lattice of the crystal is highly ordered.

Figure 4 illustrates the X-ray diffractograms based on the amount of chrysin loaded into Fe $_3$ O $_4$ @Dextran NPs.

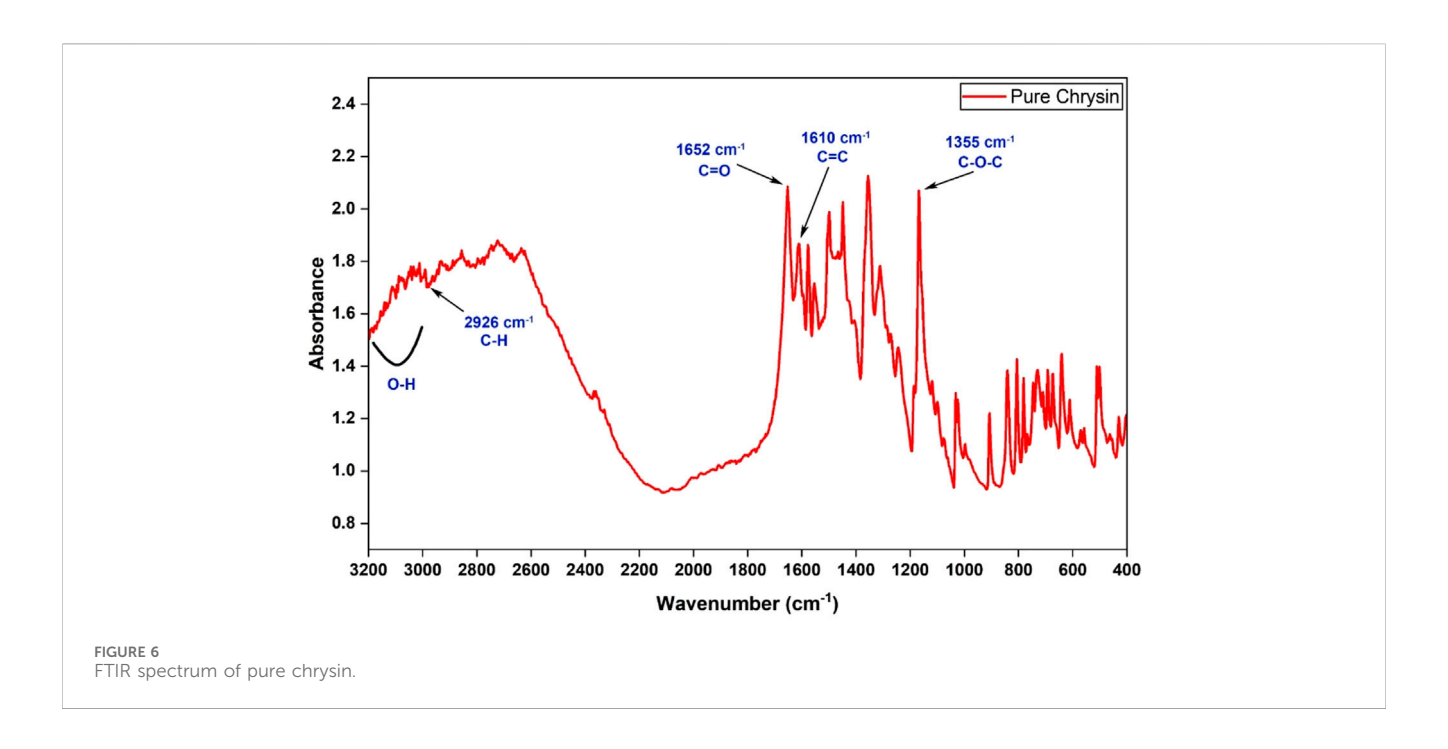
The XRD patterns of Fe₃O₄@Dextran samples loaded with varying amounts of chrysin exhibited characteristic 2θ values,

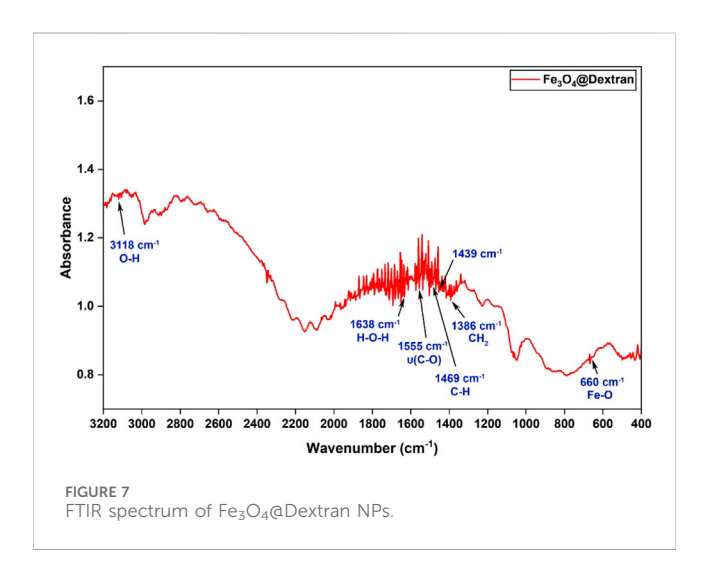


indicating the preservation of the crystalline structure upon drug loading. For Fe $_3$ O $_4$ @Dextran + D1, peaks were observed at 12.74°, 14.92°, 17.80°, 22.35°, 27.72°, 35.63°, 57.02°, and 62.78°. In contrast, Fe $_3$ O $_4$ @Dextran + D2 showed slight shifts to higher angles (e.g., 12.78°, 14.98°, 17.84°, 22.47°, 27.81°, 35.65°, 57.24°, and 62.87°). Conversely, Fe $_3$ O $_4$ @Dextran + D3 demonstrated peak shifts to slightly lower angles (e.g., 12.70°, 14.86°, 17.74°, 22.38°, 27.67°, 35.49°, 57.13°, and 62.73°). Both the drug and the NP matrix displayed peaks between 57° and 62°, confirming the successful incorporation of chrysin.

The observed peak shifts and variations suggest structural interactions between chrysin and the NP surface, influenced by the amount of drug loaded. The characteristic peaks of the drug were maintained across all samples after loading onto $Fe_3O_4@$ Dextran, although their intensity decreased. The drug molecules adsorbed to the inner surfaces of the NPs due to interactions such as hydrogen bonding or electrostatic attraction. These interactions led to slight changes in the regular crystal structure, which could lower peak intensity (Khalbas et al., 2024). Crystallite sizes (Figure 5) were determined in samples after drug loading onto $Fe_3O_4@$ Dextran NPs using Scherrer's formula (Karimova et al., 2023).

Figure 5 indicates that crystallite sizes were influenced by varying amounts of chrysin. The crystallite size of Fe_3O_4 @ Dextran NPs decreased upon drug loading, reducing from 17.1 nm (Fe_3O_4 @Dextran) to 15.69 nm (Fe_3O_4 @Dextran + D2) as the chrysin concentration doubled. An increase in drug molecules can interfere with crystallization, resulting in smaller and more finely distributed crystals (Mistry and Suryanarayanan, 2016). However, a slight increase in crystallite size was observed in Fe_3O_4 @Dextran + D3, which may result from drug molecules saturating the surface. Once the surface of the Fe_3O_4 NPs becomes saturated, additional drug molecules may affect surface energy and diminish structural strain, leading to minor crystallite growth (Li et al., 2016).





3.2 FTIR spectral analysis

FTIR spectral analysis was conducted between 3,200 and 400 cm⁻¹ to identify the functional groups within the samples. In addition to the synthesized samples, the FTIR spectrum of pure chrysin was also analyzed (Figure 6).

The absorption bands between 3,200 cm⁻¹ and 3,000 cm⁻¹ are characteristic of O-H stretching, confirming the presence of phenolic hydroxyl groups. The peak at 2,926 cm⁻¹ is assigned to C-H stretching vibrations. A prominent peak at 1,652 cm⁻¹ corresponds to the C=O stretching vibration of the flavonoid backbone, while the absorption band at 1,610 cm⁻¹ is associated with C=C aromatic stretching (Sundararajan et al., 2017; Krysa et al., 2022). Additionally, the peak at 1,355 cm⁻¹ is attributed to C-O-C stretching, indicating the presence of ether linkages. To confirm successful surface modification, dextran-coated Fe₃O₄ NPs were analyzed. The FTIR spectrum of dextran-coated Fe3O4 NPs

(Figure 7) shows absorptions at 3,118 cm $^{-1}$, 1,638 cm $^{-1}$, 1,555 cm $^{-1}$, 1,469 cm $^{-1}$, 1,386 cm $^{-1}$, and 660 cm $^{-1}$.

When compared with the literature (Lungu et al., 2025), the O-H stretching vibration of pure dextran, which is phenolic OH in glucose units, shifted to 3,118 cm⁻¹ upon coating Fe₃O₄ NPs with dextran. Concurrently, the H-O-H bending vibration associated with internal hydrogen bonding was observed at 1,638 cm⁻¹. The CH₂ deformation vibration shifted slightly to 1,386 cm⁻¹ compared to dextran. The relatively weak absorption starting from 660 cm⁻¹ is related to the Fe-O bond, indicating a metal-oxygen bond. The weak peak observed at 1,439 cm⁻¹ is also associated with the absorption caused by the interaction of dextran with Fe₃O₄, confirming the presence of dextran on the Fe₃O₄ surface. These shifts are indicative of the interaction between Fe ions and the functional groups of dextran, as well as environmental changes due to Fe-dextran coordination. The results obtained indicate that the surface of Fe₃O₄ NPs was successfully coated with dextran.

The FTIR spectra of Fe_3O_4 @Dextran NPs obtained after attaching different amounts of chrysin were compared to analyse the effect of drug loading on functional group interactions (Figure 8; see Table 1 for formulation details).

In all samples (Figures 8a-c), the changes detected in the range of 400-600 cm-1 correspond to the Fe-O stretching vibration in iron oxide NPs (Soltanpour et al., 2024). The peaks at approximately 1,380 cm⁻¹ and 1,020 cm-1 in all drugloaded samples are attributed to the C-H and C-O deformations of dextran (Bautista et al., 2005) The O-H stretching region in drug-loaded samples exhibits differences compared to the pure drug sample, indicating hydrogen bonding with the NP surface. In chrysin, the C=O peak is originally around 1,652 cm-1 (Ansari, 2008) in the drug-loaded NPs, it remains consistent, although certain modifications are observed. As shown in Figure 8a, the Fe3O4@Dextran + D1 sample exhibits a slight splitting of the C=O peak into 1,646 cm-1 and 1,637 cm-1. In Figure 8b, corresponding to the Fe3O4@Dextran + D2 sample, the C=O

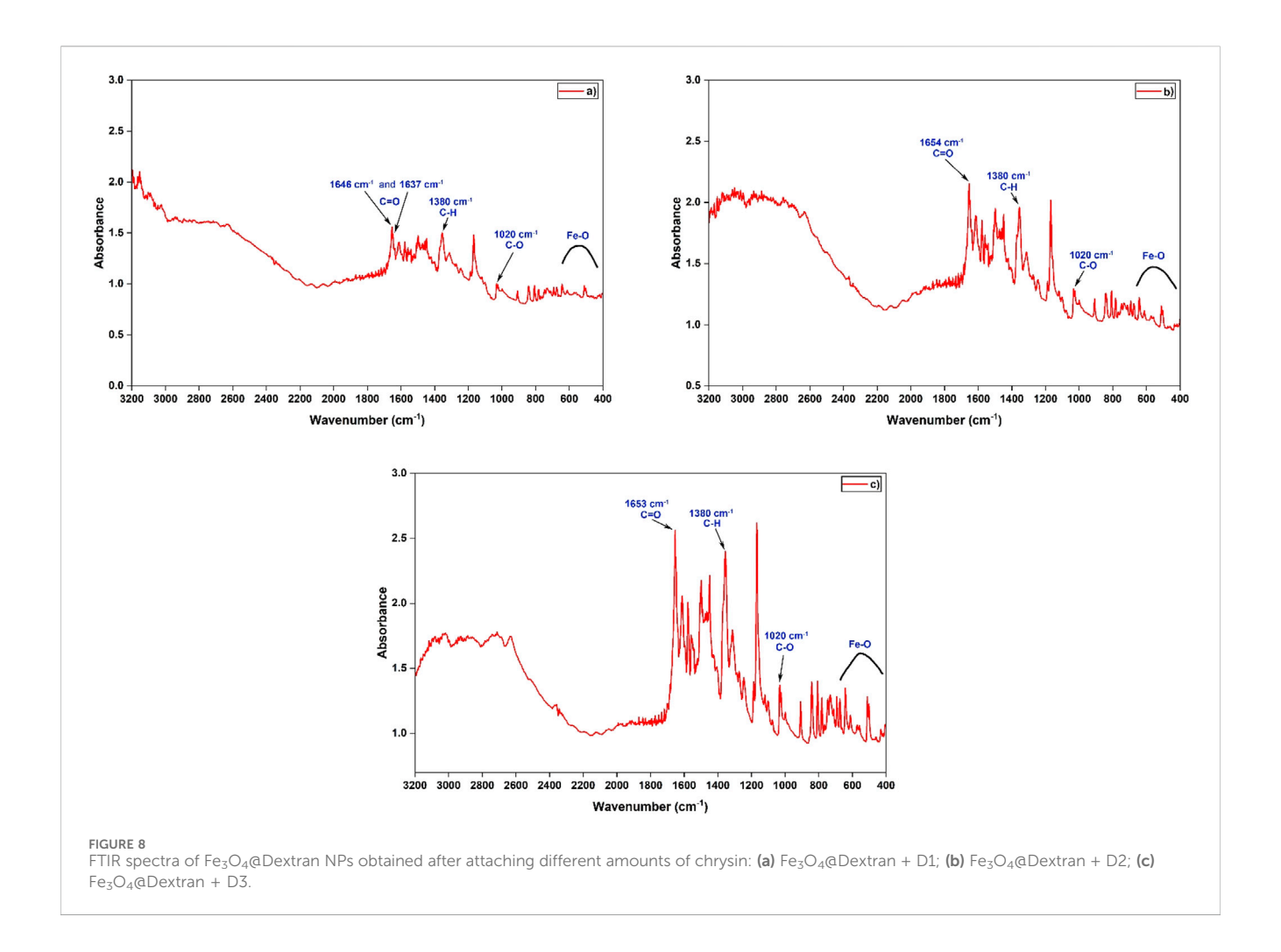
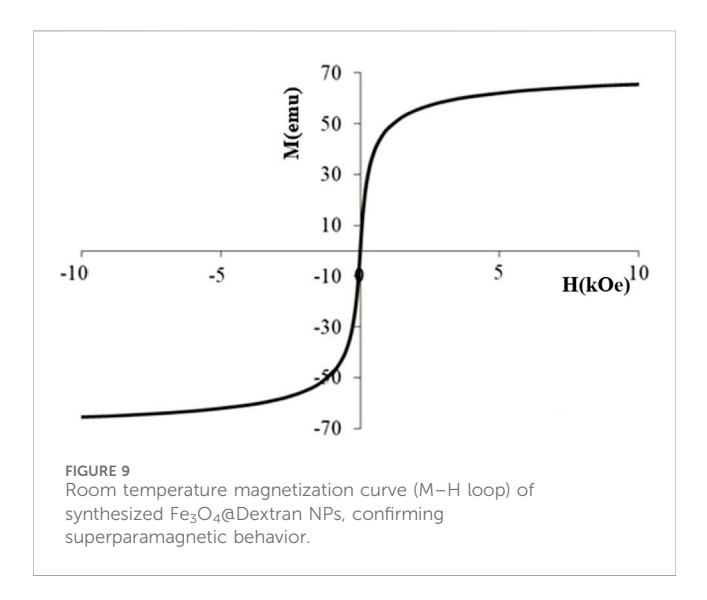


TABLE 2 Chemical bonding in the samples from FTIR wavenumber.

Bonding	Chrysin (cm ⁻¹)	Fe ₃ O ₄ @ Dextran+D1 (cm ⁻¹)	Fe ₃ O ₄ @ Dextran+D2 (cm ⁻¹)	Fe ₃ O ₄ @ Dextran+D3 (cm ⁻¹)
О-Н	3,200-3,000			
C=C	1,610			
C=O	1,652	1,646 1,637	1,654	1,653
С-Н	2,926	1,380	1,380	1,380
C-O		1,020	1,020	1,020
C-O-C	1,355			
Fe-O	-	600-400	600-400	600-400

stretching vibration peak demonstrates a small shift to 1,654 cm-1 with a more noticeable splitting, indicating a stronger interaction between chrysin and the NP surface. In Figure 8c for the Fe3O4@Dextran + D3 sample, the peak is observed at 1,653 cm-1 with the highest intensity; however, no splitting was observed, unlike in the Fe3O4@Dextran + D1 and Fe3O4@Dextran + D2 samples. This suggests that the available

binding sites in the $Fe_3O_4@Dextran + D3$ sample may have been saturated, as the drug concentration likely has exceeded the binding capacity of the NPs. This result correlates with the XRD findings, indicating that in the $Fe_3O_4@Dextran + D3$ sample iron oxide NPs were formed in a more dispersed and possibly less ordered form, further supporting the hypothesis of drug saturation and structural alteration.



Additionally, the characteristic C=C vibration of the drug at 1,610 cm⁻¹ was observed to shift slightly in all drug-loaded Fe₃O₄NPs. In the Fe₃O₄@Dextran + D1 and Fe₃O₄@Dextran + D2 samples, this peak shifts slightly to 1,616 cm⁻¹, followed by distinct band splitting. In contrast, for the Fe₃O₄@Dextran + D3 sample, the peak shifts to 1,612 cm⁻¹ without any observed splitting. Significant shifts in Fe₃O₄@Dextran + D1 and Fe₃O₄@Dextran + D2 suggest stronger interactions between the NPs and chrysin. Furthermore, the spectral regions around ~1,355 cm⁻¹ and 1,245 cm⁻¹ remain consistent across all drug-loaded samples, indicating that the structural integrity of the drug is preserved. To compare the observed absorbance in all samples, the functional bonding with wavenumbers is presented in Table 2.

Overall, the XRD, and FTIR, analyses confirm the successful incorporation of chrysin into Fe_3O_4 @Dextran NPs, while preserving structural features; NPs, and drugs exhibit strong interactions at low loading levels, whereas saturation effects become evident at higher drug concentrations.

3.3 Magnetic properties

The magnetic properties of Fe $_3$ O $_4$ @Dextran NPs were investigated at room temperature using VSM. The magnetization versus applied magnetic field (M–H) curve is presented in Figure 9, and the extracted magnetic parameters are summarized in Table 3.

The Fe $_3O_4$ @Dextran NPs exhibited a saturation magnetization (M_s) of 69.2 emu/g, a remanent magnetization (M_r) of 1.28 emu/g, and a coercivity (H_c) of 0 Oe. The squareness ratio (M_r/M_s) was calculated as 0.018. The very low squareness ratio and remanent magnetization confirm that the synthesized NPs exhibit superparamagnetic behavior at room temperature (Ganapathe et al., 2020).

3.4 UV-Vis spectral analysis

In our study, we examined the loading efficiency of the fabricated samples as a promising nanocarrier for chrysin using spectrophotometric analysis at 276.4 nm (Karimova et al., 2024). Table 4 presents the LE (%) for samples obtained with varying amounts of chrysin relative to the quantity of Fe₃O₄@Dextran NPs.

The LE (%) value for the Fe $_3$ O $_4$ @Dextran + D1 sample was 42%, which is 12% lower than that of Fe $_3$ O $_4$ @Dextran + D2 (54%) and 15% lower than that of Fe $_3$ O $_4$ @Dextran + D3 (57%). In Fe $_3$ O $_4$ @Dextran NPs, increasing the chrysin amount two-fold has minimal impact on LE (%). Several factors may contribute to this observation, including the possibility that the system is at or near saturation. For instance, diffusion limitations may hinder the system prevent drug molecules onto Fe $_3$ O $_4$ @Dextran NPs. Higher drug concentration may not facilitate the effective loading of additional drug molecules, even with high diffusion rates. Additionally, the NPs' surface may experience reduced loading capacity due to drug aggregation or precipitation at high concentrations. Consequently, increasing the drug amount may have a limited effect on loading efficiency.

To further confirmation, the UV-Vis spectra of the supernatants acquired after the loading process were recorded and are shown in Figure 10.

Pure chrysin demonstrated a strong absorption peak at 276 nm, which functioned as the reference for quantification. Compared with the spectrum of Fe_3O_4 @Dextran + D1 already showed a significant reduction in absorbance intensity, suggesting partial drug uptake by the nanocarriers, although a notable fraction of drug was still present unbound (LE = 42%). The absorbance at 276 nm revealed more stronger decrease for Fe_3O_4 @Dextran + D2, demonstrating enhanced drug incorporation and a higher loading efficiency (LE = 54%). For Fe_3O_4 @Dextran + D3, the peak intensity demonstrated only a slight additional decrease relative to Fe_3O_4 @Dextran + D2 sample, implying that the system approached saturation, with modest improvement in loading efficiency (LE = 57%). These spectral observations support the LE (%) values presented in Table 4 and provide direct evidence of the efficiency calculations.

3.5 *In-Vitro* cytotoxicity analysis

The MTT assay was employed to assess the cytotoxicity of dextran-coated Fe $_3$ O $_4$ NPs and chrysin-loaded formulations to evaluate their anti-cancer efficacy. HCT-116 colorectal cancer cells were exposed to a concentration gradient ranging from 25 µg/mL to 1 mg/mL for 24 h. The determined IC $_{50}$ value after 24 h of treatment was 16.68 µg/mL. Subsequent investigations of samples were conducted at a sub-cytotoxic concentration of 5 µg/mL, below the IC $_{50}$ threshold.

Significant cytotoxicity was observed after prolonged exposure (48–72 h); therefore, the experiment was limited to a 24-h treatment window. Cell viability results indicated that Fe_3O_4 @Dextran + D2 and Fe_3O_4 @Dextran + D3 exhibited a much greater inhibitory effect on HCT-116 cell proliferation than Fe_3O_4 @Dextran and Fe_3O_4 @Dextran + D1 at the same concentration (p = 0.0001; Figure 11).

Cell viability was significantly reduced by Fe $_3$ O $_4$ @Dextran + D2 and Fe $_3$ O $_4$ @Dextran + D3 treatments compared to the untreated control group (p < 0.0001). Furthermore, a statistically significant reduction in cell viability was observed when comparing Fe $_3$ O $_4$ @Dextran + D3 treatments to Fe $_3$ O $_4$ @Dextran + D1

TABLE 3 Magnetic parameters of synthesized Fe₃O₄@Dextran NPs.

Sample	Mr (emu/g)	Ms (emu/g)	Hc (Oe)	Square rate
Fe ₃ O ₄ @Dextran NPs	1.28	69.2	0	0.018

TABLE 4 Mathematically calculated results of chrysin LE (%) for dextrancoated and chrysin-loaded Fe $_3\text{O}_4$ NPs.

Samples	LE (%)
Fe ₃ O ₄ @Dextran + D1	42
Fe ₃ O ₄ @Dextran + D2	54
Fe ₃ O ₄ @Dextran + D3	57

(p = 0.0001). In contrast, the difference between Fe₃O₄@Dextran and Fe₃O₄@Dextran + D1 was not statistically significant (p = 0.6242). Although Fe₃O₄@Dextran + D3 exhibited greater inhibition of cell viability compared to Fe₃O₄@Dextran + D2, the difference between the two groups did not reach statistical significance (p = 0.2084).

4 Discussion

Numerous studies have reported on various drugs loaded onto functionalized NPs, demonstrating promising potential for targeted drug delivery (Ebadi et al., 2023; Karimova et al., 2024; Luong et al., 2024). Following functionalization with various coatings, these drug-loaded Fe_3O_4 NPs exhibit controlled release behavior in response to different stimuli, including pH variations, temperature sensitivity, near-infrared (NIR) laser irradiation, reactive oxygen species (ROS)-mediated cytotoxicity, DNA interactions for therapeutic effects, and low-frequency ultrasound triggers (Al Dine et al., 2017; Qi et al., 2017; Shen et al., 2018; Al Refaai et al., 2024; Cui et al., 2024).

In our study, we aimed to systematically assess the loading of chrysin onto dextran-coated Fe₃O₄ NPs at defined nanoparticle-todrug ratios (1:0.5, 1:1, and 1:2), highlighting the influence of formulation parameters on drug incorporation. A comparison of the XRD patterns of Fe₃O₄-based NPs before and after chrysin loading revealed important insights into the loading behavior and structural integrity of the core material. Following drug loading, diffraction peaks broadened and intensity decreased, particularly in the Fe₃O₄@Dextran + D1 and Fe₃O₄@Dextran + D2 samples. These characteristics suggest that the reduction in crystallinity is likely due to surface interactions or coating by chrysin molecules (Sulistyaningsih et al., 2021). The preservation of peak positions in the XRD patterns across all samples indicates that the Fe₃O₄ core structure remained stable after chrysin loading, suggesting that the drug is primarily adsorbed onto the NPs' surface rather than incorporated into the crystal lattice.

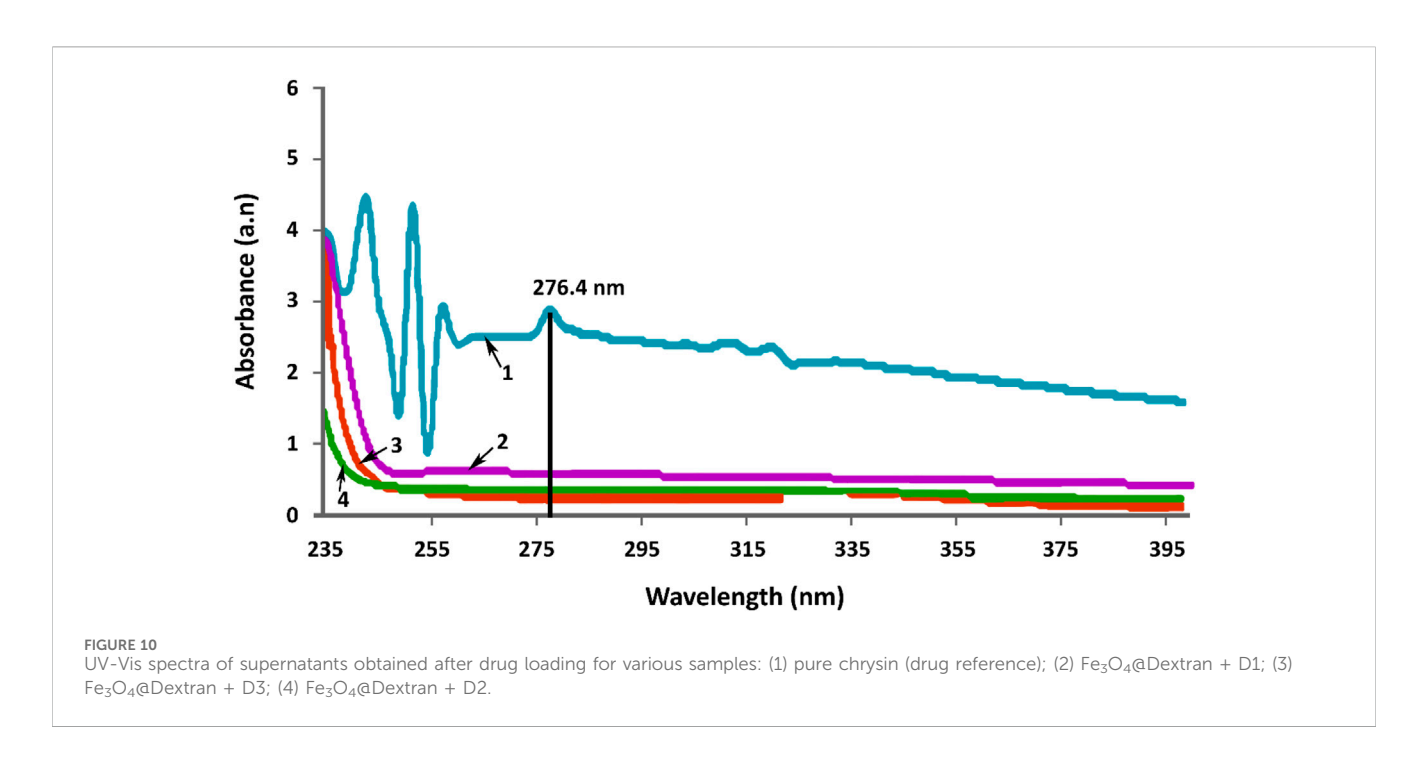
Crystallite size assessment based on the Debye–Scherrer equation, illustrated in Figure 5, demonstrated a decreasing trend: from 17.1 nm for Fe $_3$ O $_4$ @Dextran to 15.69 nm for Fe $_3$ O $_4$ @Dextran + D1, 13.7 nm for Fe $_3$ O $_4$ @Dextran + D2, and a slight increase to 14.96 nm in Fe $_3$ O $_4$ @Dextran + D3. The observed decline in crystallite size suggests that chrysin loading may limit crystal

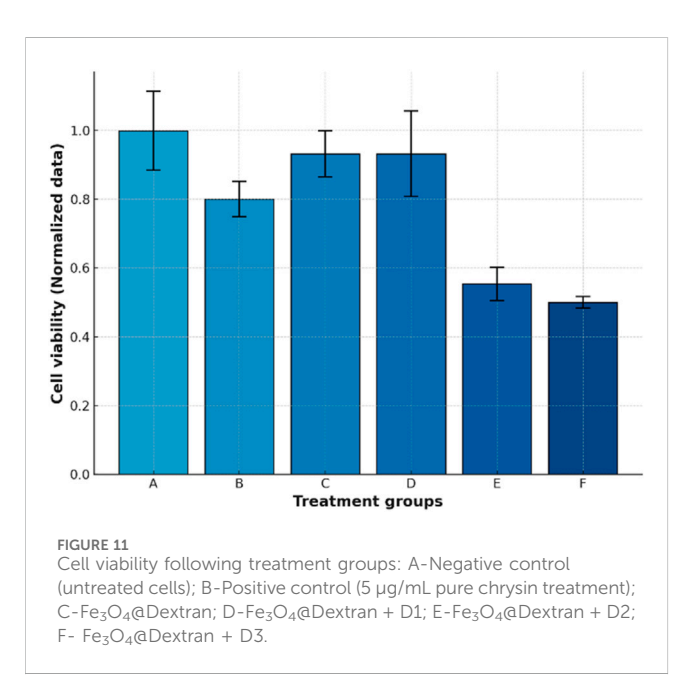
growth, potentially due to changes in surface energy or interference from drug molecules during the crystallization process (Mistry and Suryanarayanan, 2016). The minor size increase in Fe $_3$ O $_4$ @Dextran + D3 may reflect saturation of adsorption sites on the NPs' surface or modest surface relaxation effects, allowing limited growth beyond a certain drug concentration. In the Fe $_3$ O $_4$ @Dextran + D3 sample, the XRD pattern displayed negligible further differences compared to Fe $_3$ O $_4$ @Dextran + D2, indicating that the available surface sites were saturated (Najafipour et al., 2025). Consequently, the further addition of the drug caused no substantial changes in the diffraction pattern, suggesting that the maximum loading capacity had been reached.

To complement the structural findings, FTIR spectroscopy was employed to investigate the chemical interactions between the drug and the surface Of the NPs. In the FTIR spectra, the C=O stretching band (~1,650 cm⁻¹) exhibited peak splitting in Fe₃O₄@Dextran + D1 and Fe₃O₄@Dextran + D2. This splitting may result from the presence of various chemical environments surrounding the carbonyl group, including hydrogen bonding interactions between chrysin and the NP surface. In contrast, the absence of peak splitting in Fe₃O₄@Dextran + D3 suggests surface saturation, where the concentration of chrysin exceeds the number of available binding sites, leading to a more chemically uniform environment (Deeleepojananan et al., 2024). However, the absence of C=O peak splitting in Fe₃O₄@Dextran + D3 may also be influenced by factors beyond surface saturation. At higher drug concentrations, molecular aggregation could occur, potentially burying the C=O groups and reducing their accessibility for specific interactions (Narayanan et al., 2020). Additionally, reduced hydrogen bonding efficiencydue to steric hindrance or conformational constraints-may contribute to the observed spectral uniformity. These effects, either individually or in combination, could account for the presence of a single, unsplit C=O band in Fe $_3O_4$ @ $^{Dextran+}D3$.

Moreover, significant changes in the vibrations of functional groups - such as the -OH and C=O stretching bands - indicated the formation of hydrogen bonds or electrostatic interactions between chrysin and the dextran-coated surface of Fe_3O_4 NPs. The FTIR spectrum of $Fe_3O_4@Dextran + D3$ closely resembled that of $Fe_3O_4@Dextran + D2$, suggesting that the addition of excess chrysin did not result in any notable new interactions with the NPs. This observation further supports the hypothesis of surface saturation, in line with the XRD findings.

To further elucidate their physicochemical profile, magnetic characterization was conducted. The M-H hysteresis loop confirmed the superparamagnetic nature of the synthesized dextran-coated Fe $_3$ O $_4$ NPs, with a saturation magnetization (M $_s$) of 69.2 emu/g, a remanent magnetization (M $_r$) of 1.28 emu/g, and a squareness ratio (M $_r$ /M $_s$) of 0.018. The absence of coercivity and the low remanence indicate a lack of magnetic memory and aggregation, which indicates potential suitability for future biomedical applications, such as magnetically guided drug delivery, however additional evaluation will be required.





According to the LE (%) analysis, Fe_3O_4 @Dextran + D2 and Fe_3O_4 @Dextran + D3 exhibited loading efficiencies of 11% and 14%, respectively. The minimal difference in LE (%) between these samples suggests that increasing the initial drug concentration beyond a certain threshold does not significantly enhance loading efficiency. This behavior is likely due to surface saturation at higher concentrations, which limits the availability of binding sites on the NPs and reduces the efficiency of drug-NP interactions (Salahudeen and Nishtala, 2017; Najafipour et al., 2025).

The *in vitro* cytotoxicity analysis revealed distinct differences in the anticancer efficacy of the synthesized dextran-coated Fe_3O_4 -based NPs formulations. Treatment with Fe_3O_4 @Dextran + D2 and Fe_3O_4 @Dextran + D3 resulted in a statistically significant reduction

in the viability of HCT-116 colorectal cancer cells compared to both the untreated control and the unloaded Fe₃O₄@Dextran NPs (p < 0.0001). These findings confirm the role of chrysin in enhancing the therapeutic activity of the system. Furthermore, Fe₃O₄@Dextran + D1 demonstrated significantly lower cytotoxicity compared to Fe₃O₄@Dextran + D2 and Fe₃O₄@Dextran + D3 (p = 0.0001), and its effect was not statistically different from that of Fe₃O₄@Dextran NPs (p = 0.6242), suggesting limited biological efficacy. This reduced efficacy may be due to suboptimal drug loading. Interestingly, although Fe₃O₄@Dextran + D3 showed slightly higher inhibition of cell viability than Fe₃O₄@Dextran + D2, the difference was not statistically significant (p = 0.2084).

Therefore, although both formulations demonstrated effective cytotoxicity, Fe_3O_4 @Dextran + D3 did not exhibit a significant therapeutic advantage over Fe_3O_4 @Dextran + D2. Supported by XRD and FTIR analyses, Fe_3O_4 @Dextran + D2 emerges as the optimal formulation within the scope of this study, achieving efficient drug loading while preserving the structural integrity of the Fe_3O_4 core. Compared to samples with higher drug content, Fe_3O_4 @Dextran + D2 maintains a favorable balance - surface saturation has not yet occurred, enabling strong chrysin adsorption that effectively limits crystal growth without compromising nanoparticle crystallinity. In contrast, formulations with increased drug loading exhibit signs of surface saturation, as indicated by minimal changes in crystallite size and diffraction patterns, suggesting limited additional drug binding.

Based on the combined results from XRD, FTIR, and loading efficiency analyses, Fe $_3$ O $_4$ @Dextran NPs demonstrate structural stability and effective drug-loading capability, with chrysin adsorbed onto their surface. The promising *in vitro* cytotoxicity results demonstrate that this nanomaterial holds potential for future anticancer strategies, while its magnetic properties offer opportunities for theragnostic applications. Functionalized Fe $_3$ O $_4$ NPs can accumulate at cancer cell sites through the enhanced permeability and retention (EPR) effect, potentially reducing

toxic side effects and improving therapeutic efficacy (Chehelgerdi et al., 2023). However, this work remains at a fundamental stage, and further studies - including *in vivo* evaluation, biodistribution and clearance kinetics, systemic toxicity evaluations, and long-term stability testing - will be necessary to examine their feasibility for clinical applications.

Altogether, our findings highlight Fe $_3$ O $_4$ @Dextran + D2 as a promising model system for further investigation. This work offers valuable insights into the structure -function relationships of drugloaded Fe $_3$ O $_4$ nanomaterials and lays the groundwork for future research aimed at advancing theranostic applications. However, considerable optimization and additional studies are still necessary before clinical translation can be realistically pursued.

Data availability statement

The raw data supporting the conclusions of this article will be made available by the authors, without undue reservation.

Ethics statement

Ethical approval was not required for the studies on humans in accordance with the local legislation and institutional requirements because only commercially available established cell lines were used.

Author contributions

AK: Validation, Conceptualization, Writing – review and editing, Data curation, Writing – original draft, Visualization, Formal Analysis. SH: Writing – original draft, Formal Analysis, Investigation. HS: Visualization, Writing – review and editing, Conceptualization. SN: Investigation, Writing – review and editing. LG: Writing – review and editing, Investigation. AM: Writing – review and editing, Visualization. GE: Formal Analysis, Writing – review and editing. TS: Writing – review and editing,

References

Akbarzadeh, A., Samiei, M., and Davaran, S. (2012). Magnetic nanoparticles: preparation, physical properties, and applications in biomedicine. *Nanoscale Res. Lett.* 7, 144–13. doi:10.1186/1556-276x-7-144

Al Dine, E. J., Ferjaoui, Z., Ghanbaja, J., Roques-Carmes, T., Meftah, A., Hamieh, T., et al. (2017). Thermo-responsive magnetic Fe3O4@ P (MEO2MAX-OEGMA100-X) NPs and their applications as drug delivery systems. *Int. J. Pharm.* 532 (2), 738–747. doi:10.1016/j.ijpharm.2017.09.019

Al Refaai, K. A., AlSawaftah, N. A., Abuwatfa, W., and Husseini, G. A. (2024). Drug release via ultrasound-activated nanocarriers for cancer treatment: a review. *Pharmaceutics* 16 (11), 1383. doi:10.3390/pharmaceutics16111383

Ali, A., Shah, T., Ullah, R., Zhou, P., Guo, M., Ovais, M., et al. (2021). Review on recent progress in magnetic nanoparticles: synthesis, characterization, and diverse applications. *Front. Chem.* 9, 629054. doi:10.3389/fchem.2021.629054

Ansari, A. A. (2008). DFT and 1H NMR molecular spectroscopic studies on biologically anti-oxidant active paramagnetic lanthanide (III)-chrysin complexes. *Main. Group Chem.* 7 (1), 43–56. doi:10.1080/10241220801912637

Attanayake, S. B., Nguyen, M. D., Chanda, A., Alonso, J., Orue, I., Lee, T. R., et al. (2025). Superparamagnetic superparticles for magnetic hyperthermia therapy: overcoming the particle size limit. *ACS Appl. Mater. and Interfaces* 17 (13), 19436–19445. doi:10.1021/acsami.4c22386

Visualization, Software. NL: Formal Analysis, Writing – review and editing. IN: Data curation, Writing – review and editing. CR: Project administration, Supervision, Writing – review and editing. VY: Writing – review and editing, Visualization, Project administration.

Funding

The author(s) declare that no financial support was received for the research and/or publication of this article.

Conflict of interest

The authors declare that the research was conducted in the absence of any commercial or financial relationships that could be construed as a potential conflict of interest.

Generative AI statement

The author(s) declare that no Generative AI was used in the creation of this manuscript.

Any alternative text (alt text) provided alongside figures in this article has been generated by Frontiers with the support of artificial intelligence and reasonable efforts have been made to ensure accuracy, including review by the authors wherever possible. If you identify any issues, please contact us.

Publisher's note

All claims expressed in this article are solely those of the authors and do not necessarily represent those of their affiliated organizations, or those of the publisher, the editors and the reviewers. Any product that may be evaluated in this article, or claim that may be made by its manufacturer, is not guaranteed or endorsed by the publisher.

Baldelli, E., Subramanian, M., Alsubaie, A. M., Oldaker, G., Emelianenko, M., El Gazzah, E., et al. (2021). Heterogeneous off-target effects of ultra-low Dose Dimethyl Sulfoxide (DMSO) on targetable signaling events in lung cancer *in vitro* models. *Int. J. Mol. Sci.* 22 (6), 2819. doi:10.3390/ijms22062819

Bautista, M. C., Bomati-Miguel, O., del Puerto Morales, M., Serna, C. J., and Veintemillas-Verdaguer, S. (2005). Surface characterisation of dextran-coated iron oxide nanoparticles prepared by laser pyrolysis and coprecipitation. *J. Magnetism Magnetic Mater.* 293 (1), 20–27. doi:10.1016/j.jmmm.2005.01.038

Chehelgerdi, M., Chehelgerdi, M., Allela, O. Q. B., Pecho, R. D. C., Jayasankar, N., Rao, D. P., et al. (2023). Progressing nanotechnology to improve targeted cancer treatment: overcoming hurdles in its clinical implementation. *Mol. cancer* 22 (1), 169. doi:10.1186/s12943-023-01865-0

Chuan Lim, E. W., and Feng, R. (2012). Agglomeration of magnetic nanoparticles. J. Chem. Phys. 136 (12), 124109. doi:10.1063/1.3697865

Cui, J., Cai, X., Qian, R., Wu, L., Qi, X., Cao, J., et al. (2024). Tween 80 micelles loaded with Fe3O4 nanoparticles and artemisinin for combined oxygen-independent ferroptosis therapy of cancer. *Pharmaceutics* 16 (5), 639. doi:10.3390/pharmaceutics16050639

Deeleepojananan, C., Zhou, J., and Grassian, V. H. (2024). Heterogeneous interactions and transformations of dibasic esters with indoor relevant surfaces. *Environ. Sci. Process. and Impacts* 26 (3), 582–594. doi:10.1039/d3em00542a

Ebadi, M., Rifqi Md Zain, A., Tengku Abdul Aziz, T. H., Mohammadi, H., Tee, C. A. T., and Rahimi Yusop, M. (2023). Formulation and characterization of Fe3O4@ PEG nanoparticles loaded sorafenib; molecular studies and evaluation of cytotoxicity in liver cancer cell lines. *Polymers* 15 (4), 971. doi:10.3390/polym15040971

- Ezealigo, U. S., Ezealigo, B. N., Aisida, S. O., and Ezema, F. I. (2021). Iron oxide nanoparticles in biological systems: Antibacterial and toxicology perspective. *JCIS Open* 4, 100027. doi:10.1016/j.jciso.2021.100027
- Ganapathe, L. S., Mohamed, M. A., Mohamad Yunus, R., and Berhanuddin, D. D. (2020). Magnetite (Fe3O4) nanoparticles in biomedical application: from synthesis to surface functionalisation. *Magnetochemistry* 6 (4), 68. doi:10.3390/magnetochemistry6040068
- Huang, J., Li, Y., Orza, A., Lu, Q., Guo, P., Wang, L., et al. (2016). Magnetic nanoparticle facilitated drug delivery for cancer therapy with targeted and imageguided approaches. *Adv. Funct. Mater.* 26 (22), 3818–3836. doi:10.1002/adfm. 201504185
- Ji, Y., and Wang, C. (2023). Magnetic iron oxide nanoparticle-loaded hydrogels for photothermal therapy of cancer cells. *Front. Bioeng. Biotechnol.* 11, 1130523. doi:10. 3389/fbioe.2023.1130523
- Karimova, A., Shirinova, H., Nargiz, G., Nuriyeva, S., and Gahramanli, L. (2023). Preparation and characterization of magnetic iron oxide (Fe3O4) nanoparticles with different polymer coating agents.
- Karimova, A., Hajizada, S., Shirinova, H., Nuriyeva, S., Gahramanli, L., Yusuf, M. M., et al. (2024). Surface modification strategies for chrysin-loaded iron oxide nanoparticles to boost their anti-tumor efficacy in human colon carcinoma cells. *J. Funct. Biomaterials* 15 (2), 43. doi:10.3390/jfb15020043
- Kaur, H., Singh Malik, D., and Kaur, G. (2015). Enhanced dissolution and antioxidant activity of chrysin nanoparticles employing co-precipitation as a technique. *Pharm. Nanotechnol.* 3 (3), 205–218. doi:10.2174/2211738504666151127192541
- Khalbas, A. H., Albayati, T. M., Ali, N. S., and Salih, I. K. (2024). Drug loading methods and kinetic release models using of mesoporous silica nanoparticles as a drug delivery system: a review. *South Afr. J. Chem. Eng.* 50, 261–280. doi:10.1016/j.sajce.2024. 08.013
- Krysa, M., Szymańska-Chargot, M., and Zdunek, A. (2022). FT-IR and FT-Raman fingerprints of flavonoids–a review. *Food Chem.* 393, 133430. doi:10.1016/j.foodchem. 2022.133430
- Li, Y., Yu, Y., Wang, H., and Zhao, F. (2016). Effect of process parameters on the recrystallization and size control of puerarin using the supercritical fluid antisolvent process. *asian J. Pharm. Sci.* 11 (2), 281–291. doi:10.1016/j.ajps.2015.12.001
- Li, Y., Chen, J., Xia, Q., Shang, J., He, Y., Li, Z., et al. (2024). Photothermal Fe3O4 nanoparticles induced immunogenic ferroptosis for synergistic colorectal cancer therapy. *J. Nanobiotechnology* 22 (1), 630. doi:10.1186/s12951-024-02909-3
- Liu, S., Yu, B., Wang, S., Shen, Y., and Cong, H. (2020). Preparation, surface functionalization and application of Fe3O4 magnetic nanoparticles. *Adv. colloid Interface Sci.* 281, 102165. doi:10.1016/j.cis.2020.102165
- Lungu, I., Potlog, T., Airinei, A., Tigoianu, R., and Gherasim, C. (2025). Exploring the Photophysical properties of Some dextran-iron oxide nanoparticle Composites. *Molecules* 30 (11), 2290. doi:10.3390/molecules30112290
- Luong, H. V. T., Diep, M. T., Nguyen, N. Y., Pham, D. T., Cao, L. N. H., and Ha, T. M. P. (2024). Alginate–functionalized Fe3O4 nanoparticles as a drug delivery system for targeted controlled release. *J. Drug Deliv. Sci. Technol.* 93, 105465. doi:10.1016/j.jddst. 2024.105465
- Mamani, J. B., Borges, J. P., Rossi, A. M., and Gamarra, L. F. (2023). Magnetic nanoparticles for therapy and diagnosis in nanomedicine. *Pharm.* 15 (6), 1663. doi:10. 3390/pharmaceutics15061663
- Mistry, P., and Suryanarayanan, R. (2016). Strength of drug-polymer interactions: implications for crystallization in dispersions. *Cryst. Growth and Des.* 16 (9), 5141–5149. doi:10.1021/acs.cgd.6b00714
- Mosayebi, J., Kiyasatfar, M., and Laurent, S. (2017). Synthesis, functionalization, and design of magnetic nanoparticles for theranostic applications. *Adv. Healthc. Mater.* 6 (23), 1700306. doi:10.1002/adhm.201700306
- Najafipour, I., Emami, N., Sadeh, P., Amoli, A., Mosleh-Shirazi, S., Amani, A. M., et al. (2025). Synthesis of Fe3O4@ MIL-101-OH/Chitosan for adsorption and release of doxorubicin. *Polym. Test.* 142, 108659. doi:10.1016/j.polymertesting.2024.108659

- Narayanan, P., Swami, K. R., Prathibha, T., and Venkatesan, K. (2020). FTIR spectroscopic investigations on the aggregation behaviour of N, N, N', N'- tetraoctyldiglycolamide and N, N-dioctylhydroxyacetamide in n-dodecane during the extraction of Nd (III) from nitric acid medium. *J. Mol. Liq.* 314, 113685. doi:10.1016/j.molliq.2020.113685
- Pozzi, M., Jonak Dutta, S., Kuntze, M., Bading, J., Rußbult, J. S., Fabig, C., et al. (2024). Visualization of the high surface-to-volume ratio of nanomaterials and its consequences. *J. Chem. Educ.* 101 (8), 3146–3155. doi:10.1021/acs.jchemed.4c00089
- Pusta, A., Tertis, M., Crăciunescu, I., Turcu, R., Mirel, S., and Cristea, C. (2023). Recent advances in the development of drug delivery applications of magnetic nanomaterials. *Pharmaceutics* 15 (7), 1872. doi:10.3390/pharmaceutics15071872
- Qi, X., Xiong, L., Peng, J., and Tang, D. (2017). Near infrared laser-controlled drug release of thermoresponsive microgel encapsulated with Fe 3 O 4 nanoparticles. *Rsc Adv.* 7 (32), 19604-19610. doi:10.1039/c7ra01009e
- Ramazanov, M. A., Maharramov, A. M., Ali-zada, R. A., Shirinova, H. A., and Hajiyeva, F. V. (2020). Theoretical and experimental investigation of the particle size distribution and magnetic properties of the PP+ FE3O4 nanocomposites. *J. Thermoplast. Compos. Mater.* 33 (1), 125–137. doi:10.1177/0892705718804578
- Ramazanov, M., Karimova, A., and Shirinova, H. (2021). Magnetism for drug delivery, MRI and hyperthermia applications: a review. *Biointerface Res. Appl. Chem.* 11 (2), 8654–8668. doi:10.33263/BRIAC112.86548668
- Sala, K., Cholewa, K., Bańkosz, M., and Tyliszczak, B. (2023). Analysis of surface and physicochemical properties of Novel hydrogel materials supported with magnetic nanoparticles. *Coatings* 13 (11), 1907. doi:10.3390/coatings13111907
- Salahudeen, M. S., and Nishtala, P. S. (2017). An overview of pharmacodynamic modelling, ligand-binding approach and its application in clinical practice. *Saudi Pharm. J.* 25 (2), 165–175. doi:10.1016/j.jsps.2016.07.002
- Shen, L., Li, B., and Qiao, Y. (2018). Fe3O4 nanoparticles in targeted drug/gene delivery systems. Materials~11~(2),~324.~doi:10.3390/ma11020324
- Soltanpour, P., Naderali, R., and Mabhouti, K. (2024). Comparative study on structural, morphological, and optical properties of MS/Fe3O4 nanocomposites and M-doped Fe3O4 nanopowders (M= Mn, Zn). Sci. Rep. 14 (1), 21287. doi:10.1038/s41598-024-72026-6
- Sood, A., Mehrotra, A., Sharma, U., Aggarwal, D., Singh, T., Shahwan, M., et al. (2024). Advancements and recent explorations of anti-cancer activity of chrysin: from molecular targets to therapeutic perspective. *Explor. Target. Anti-tumor Ther.* 5 (3), 477–494. doi:10.37349/etat.2024.00230
- Stiufiuc, G. F., and Stiufiuc, R. I. (2024). Magnetic nanoparticles: synthesis, characterization, and their use in biomedical field. *Appl. Sci.* 14 (4), 1623. doi:10. 3390/app14041623
- Sulistyaningsih, T., Ariyani, S., and Astuti, W. (2021). "Preparation of magnetite coated humic acid (Fe3O4-HA) as malachite green dye adsorbent," in *Journal of Physics: Conference Series* (IOP Publishing).
- Sundararajan, M., Thomas, P. A., Venkadeswaran, K., Jeganathan, K., and Geraldine, P. (2017). Synthesis and characterization of chrysin-loaded β -cyclodextrin-based nanosponges to enhance *in-vitro* solubility, photostability, drug release, antioxidant effects and antitumorous efficacy. *J. Nanosci. Nanotechnol.* 17 (12), 8742–8751. doi:10. 1166/jnn.2017.13911
- Wu, W., Wu, Z., Yu, T., Jiang, C., and Kim, W.-S. (2015). Recent progress on magnetic iron oxide nanoparticles: synthesis, surface functional strategies and biomedical applications. *Sci. Technol. Adv. Mater.* 16 (2), 023501. doi:10.1088/1468-6996/16/2/023501
- Yan, H., Zhang, J.-c., You, C.-x., Song, Z.-w., Yu, B.-w., and Shen, Y. (2009). Surface modification of Fe3O4 nanoparticles and their magnetic properties. *Int. J. Minerals, Metallurgy Mater.* 16 (2), 226–229. doi:10.1016/s1674-4799(09)60038-8
- $\label{eq:continuous} Zein, R., Sharrouf, W., and Selting, K. (2020). Physical properties of nanoparticles that result in improved cancer targeting. \textit{J. Oncol.} 2020 (1), 1–16. doi:10.1155/2020/5194780$
- Zhang, C., Deng, Y., Dai, H., Zhou, W., Tian, J., Bing, G., et al. (2017). Effects of dimethyl sulfoxide on the morphology and viability of primary cultured neurons and astrocytes. *Brain Res. Bull.* 128, 34–39. doi:10.1016/j.brainresbull.2016.11.004
- Zhu, N., Ji, H., Yu, P., Niu, J., Farooq, M., Akram, M. W., et al. (2018). Surface modification of magnetic iron oxide nanoparticles. *Nanomaterials* 8 (10), 810. doi:10. 3390/nano8100810